Journal of Environmental Engineering and Energy

www.jeee.reapress.com

J. Environ. Eng. Energy Vol. 2, No. 2 (2025) 118–140.

Paper Type: Original Article

Comparative Analysis of Thermal Performance in Battery Cells with Different Materials within a PCM-Based Passive Thermal Management System

Mehdi Mohammadkhani*

Faculty of Mechanical & Energy Engineering, Shahid Beheshti University, Tehran, Iran; m_mohammadkhani@sbu.ac.ir.

Citation:

Received: 26 December 2024 *Revised: 12 February 2025* *Accepted: 02 April 2025*	Mohammadkhani, M., & Jahangiri, A. (2025). Comparative analysis of thermal performance in battery cells with different materials within a PCM-based passive thermal management system. *Journal of Environmental Engineering and Energy, 2*(2), 118-140.

Abstract

This paper investigates the thermal performance of Lithium-Ion Batteries (LIB), Lithium-Sulfur (Li-S), and Sodium-Ion Batteries (SIB) batteries with integrated Phase Change Materials (PCMs) at discharge rates of 1C, 2C, 3C, and 4C. Using ANalysis SYStem (ANSYS) simulations, the study analyzes static temperature distribution to evaluate the effectiveness of PCM cooling. Results show that LIB batteries perform well under moderate discharge rates but require enhanced cooling at higher rates. Li-S batteries struggle with localized overheating due to low thermal conductivity, highlighting the need for improved PCM designs. SIB demonstrate superior thermal stability, with PCM effectively managing heat even at higher rates. This study emphasizes the importance of tailored thermal management. It suggests further optimization of PCM systems to enhance the efficiency and safety of next-generation batteries for energy storage and electric vehicle applications.

Keywords: Battery thermal management, Phase change materials, Lithium-ion batteries, Lithium-sulfur batteries, Sodium-ion batteries, Thermal conductivity, Energy storage.

1 | Introduction

Electric Vehicles (EVs) have emerged as a cornerstone of sustainable transportation, driven by rapid advancements in battery technology. Among various energy storage options, Lithium-Ion Batteries (LIBs) remain the dominant choice due to their high energy density, safety, and long cycle life. However, the push for next-generation chemistries, such as Lithium-Sulfur (Li-S), Sodium-Ion Batteries (SIBs), and All-Solid-State Batteries (ASSBs), reflects the industry's pursuit of greater efficiency and cost-effectiveness.

Corresponding Author: m_mohammadkhani@sbu.ac.ir

https://doi.org/10.22105/jeee.v2i2.41

Battery performance is highly sensitive to operating temperature, as excessive heat can accelerate degradation, capacity loss, and thermal runaway risks. To mitigate these issues, effective Thermal Management Systems (TMS) are essential for maintaining optimal performance and safety. This study explores the interplay between battery materials and their cooling requirements, with a particular emphasis on Phase Change Materials (PCMs) as a promising passive thermal management solution.

1.1 | Battery Materials in Electric Vehicles

Modern EV energy storage solutions rely on several battery chemistries, each offering unique advantages and challenges.

1.1.1 | Lithium-Ion batteries

LIB are the dominant energy storage technology in EVs, favored for their high energy density, scalability, and well-established manufacturing processes [1], [2]. LIB chemistries such as Nickel Manganese Cobalt Oxide (NMC) and Lithium Iron Phosphate (LFP) offer distinct trade-offs:

I. NMC batteries provide higher energy density, making them suitable for long-range EVs.

II. LFP batteries exhibit superior thermal stability and cycle life, reducing safety concerns.

Despite their advantages, LIBs face challenges such as capacity fading, dendrite formation, and sensitivity to high temperatures, necessitating robust thermal management solutions [3–6]. Advanced modeling approaches, such as physics-based simulations, provide insights into heat generation mechanisms and guide the development of optimized cooling strategies [7], [8].

1.1.2 | Lithium-Sulfur batteries

Li-S batteries represent a significant leap in energy storage technology, with theoretical energy densities exceeding those of LIBs [9], [10]. However, widespread adoption remains hindered by the polysulfide shuttle effect, capacity fading, and volumetric expansion during charge-discharge cycles [11], [12]. Research efforts focus on cathode design, electrolyte optimization, and Layered Double Hydroxides (LDHs) as separators to enhance cycling stability and mitigate thermal challenges [13–15].

1.1.3 | Sodium-Ion batteries

SIBs are gaining traction as a low-cost alternative to LIBs, leveraging the abundance of sodium and simplified manufacturing [16], [17]. While SIBs exhibit lower energy densities, advancements in electrode materials and electrolyte formulations have improved their thermal stability and lifespan, making them viable for stationary energy storage applications [18], [19].

1.2 | Cooling Requirements for Battery Systems

High-performance batteries generate heat during charge and discharge cycles due to electrochemical reactions and internal resistance [5], [20]. Excessive temperature rise can lead to thermal runaway, posing safety risks, particularly in EV applications where high-power densities are involved [6], [21]. Effective thermal management strategies are crucial to:

I. Optimize battery efficiency by maintaining temperatures within the ideal operating range (15–45°C) [22], [23].

II. Minimize thermal gradients that contribute to uneven aging and capacity degradation [24], [25].

III. Prevent catastrophic failure due to thermal runaway [26].

The role of effective TMS, particularly for EVs, is critical for battery longevity and safety [27]. Additionally, battery degradation mechanisms—such as Solid Electrolyte Interface (SEI) formation and lithium plating—are closely linked to thermal behavior, further highlighting the importance of adaptive TMS solutions [28–30].

1.3 | Thermal Management Systems

To address thermal challenges, several battery cooling techniques have been developed, ranging from air and liquid cooling to advanced PCM-based and hybrid systems.

1.3.1 | Air-cooling

Air-cooling, including natural and forced convection, is a cost-effective and lightweight solution for battery temperature regulation [23]. Modified airflow channels and fin structures can enhance heat dissipation efficiency [31], [32]. However, air cooling has limited heat transfer capacity, making it insufficient for high-performance EV applications [33].

1.3.2 | Liquid cooling

Liquid cooling offers superior heat dissipation and temperature uniformity, making it the preferred choice for high-performance EVs [23], [34]. Cold plates and serpentine channels are commonly used to optimize coolant flow and reduce thermal gradients [35]. Despite its effectiveness, complexity and maintenance requirements remain key challenges.

1.3.3 | Phase change material cooling

PCM-based cooling systems utilize the high latent heat of fusion to absorb and dissipate thermal energy during phase transitions [36], [37]. Several strategies for enhancing PCM-based TMS have been reviewed, including the incorporation of nano-enhanced PCMs and advanced cooling configurations, offering valuable insights into improving heat dissipation efficiency [38]. Improvements in PCM thermal conductivity and the integration of additional techniques such as extended surfaces (fins) have been suggested to overcome the limitations of PCM cooling systems, particularly for green vehicle applications [39]. Common PCMs include paraffin wax and composite PCMs with enhanced thermal conductivity [40], [41]. While PCM-based solutions excel in passive cooling applications, they suffer from low thermal conductivity and potential material leakage, necessitating further optimization. Nano-enhanced PCMs have demonstrated promising improvements in thermal performance and stability [37].

1.3.4 | Hybrid cooling systems

Although PCM cooling systems have proven effective for LI and SIB, hybrid solutions combining active and passive cooling systems show potential for even greater temperature regulation efficiency, particularly for systems with high thermal loads [42]. Hybrid systems integrate active and passive cooling methods, combining PCMs with liquid cooling or heat pipes to enhance temperature regulation [23]. Recent advancements, such as nano-enhanced PCMs and thermoelectric elements, have demonstrated significant potential in maintaining temperature uniformity under high-discharge conditions [41], [42].

Advancements in battery materials and thermal management technologies are shaping the future of EV energy storage. While LIBs remain the dominant choice, next-generation chemistries such as Li-S, SIBs, and ASSBs promise greater energy efficiency and sustainability. Effective TMS are crucial for harnessing their full potential.

Among available cooling strategies, PCM-based systems stand out for their simplicity and efficiency in maintaining optimal operating conditions. However, further research is needed to overcome their limitations, particularly low thermal conductivity and material stability. The integration of hybrid cooling systems, combining PCMs with advanced cooling techniques, offers a promising pathway toward safer, more efficient, and scalable thermal management solutions for EV applications.

2 | Methodology

2.1 | Battery Modeling in ANalysis SYStem

Battery modeling plays a fundamental role in evaluating the thermal and electrical performance of different battery chemistries. In this study, LIB, Li-S, and SIB were modeled using ANalysis SYStem (ANSYS) to analyze their behavior under varying thermal and electrical conditions. Each battery type was designed with a nominal capacity of 14.6 Ah, and the simulations assumed constant heat generation during discharge at fixed C-rates, as referenced in [1]. The objective of this modeling was to assess heat generation, current density distribution, and DOD variations to gain insight into the performance of each battery chemistry.

The geometries of the battery cells were carefully designed based on their respective electrochemical properties and standard industry specifications. *Fig. 1* illustrates the battery cell design, where part a presents the dimensional layout of the battery, including electrode and terminal placement, and part b depicts the 3D representation of the battery cell model in ANSYS. The model accurately captures the key internal components, including planar electrodes, electrolyte layers, separators, and terminals. These elements were integrated into the simulation to ensure a realistic representation of the battery's behavior under different discharge conditions.

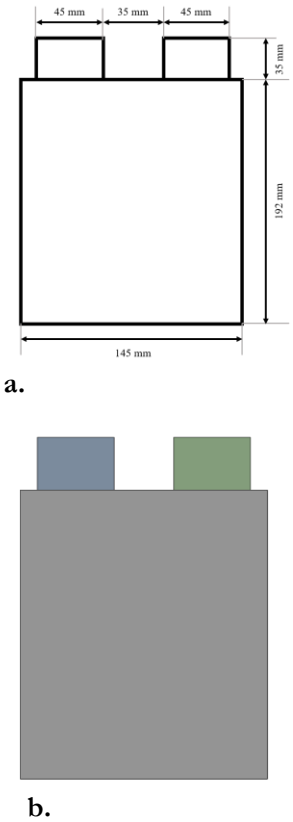

Fig. 1. Battery cell geometry and numerical model; a. Dimensions of the battery cell, and b. Battery cell model in ANSYS software.

To obtain meaningful results, a high-fidelity 3D numerical model was developed for each battery type. The models were constructed using reference data from prior studies, particularly those analyzing thermal gradients, heat generation, and electrochemical behavior in energy storage systems. The primary objective was to investigate the interactions between heat dissipation, current density distribution, and the DOD, which are critical factors in determining the efficiency and longevity of a battery. Furthermore, the study aimed to compare how different battery materials respond to thermal stress and to evaluate their suitability for applications in EVs and energy storage systems.

To ensure accuracy and computational efficiency, a refined meshing strategy was employed. The meshing process was designed to optimize the balance between solution accuracy and computational cost, with 94,470 nodes and 61,980 elements used for each simulation. Mesh refinement was concentrated in regions where heat generation and current flow density were highest, ensuring that these areas were adequately resolved to capture thermal variations and electrochemical performance accurately. The applied meshing technique allowed for precise evaluation of temperature distribution, electrical conductivity, and localized heating effects within the battery cells while maintaining a feasible computational workload.

This modeling approach provided essential insights into the thermal and electrical behavior of LIBs, Li-S batteries, and SIBs, facilitating a comparative assessment of their performance under identical operating conditions. The findings contributed to optimizing battery designs by identifying potential thermal hotspots and inefficiencies, which are crucial for improving battery cooling strategies and extending their operational lifespan.

2.2 | Phase Change Materials Implementation

PCMs are widely used in battery TMS to regulate excessive heat generation during charging and discharging cycles. Effective thermal management is crucial for preventing thermal runaway, uneven temperature distribution, and performance degradation in high-energy-density batteries. In this study, PCM was applied around the battery cell with a uniform thickness of 5 mm on all sides except the top, as shown in *Fig. 2*. This configuration was chosen to maximize heat absorption while minimizing additional weight and material usage.

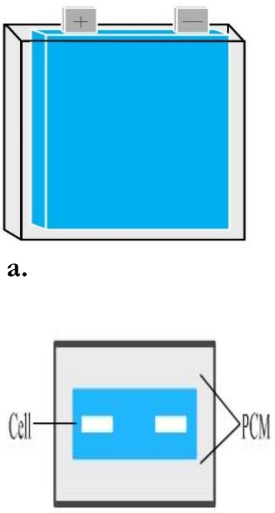

Fig. 2. PCM integration around the battery cell; a. Side view of the battery cell model with PCM material, b. Top view illustrating the placement of PCM material around the battery cell.

During operation, the heat generated by the battery is transferred to the PCM through conduction. The solid PCM absorbs heat primarily via conduction until melting begins, at which point convection mechanisms start playing a role in heat transfer within the liquid PCM phase. The inclusion of aluminum fins further enhances heat dissipation by conducting heat away from both solid and liquid PCM and transferring it to the battery containment tube, which ultimately dissipates the heat to the surroundings. Additionally, convection between the PCM and air at the top boundary ensures that excess heat is dissipated naturally. The side and bottom boundaries of the PCM layer are insulated, ensuring that heat flow is directed outward.

To model these complex heat transfer interactions, a detailed numerical simulation was performed in ANSYS Fluent, incorporating governing equations for continuity, momentum, turbulence, and energy conservation. The Volume of Fluid (VOF) multiphase model was employed to track the moving interface between PCM

and air during phase transition. The PISO pressure-velocity coupling method was selected to ensure computational efficiency, as it has been shown to produce results comparable to the SIMPLE method while requiring fewer computational resources.

2.2.1|Governing equations for phase change materials thermal behavior

The governing equations for PCM thermal behavior in this study are based on reference [43], which outlines the continuity, momentum, and energy conservation equations used to model heat transfer in PCM-based Battery Thermal Management Systems (BTMS). The equations account for conduction, convection, and phase change processes, while the multiphase VOF model simulates the evolving interface between PCM and air, as well as the liquid fraction during melting.

I. Continuity equation.

The continuity equation ensures mass conservation by tracking the volume fraction of each phase within a control volume:

$$\frac{D\alpha_n}{Dt} = 0, \tag{1}$$

where α_n represents the volume fraction of the nth fluid in the computational cell. This equation helps determine the phase presence of PCM and air in different regions of the simulation.

II. Momentum equation.

The momentum equation, which governs the velocity field and fluid motion within the PCM, is given as:

$$\rho\frac{D\vec{V}}{Dt} = -\nabla p + \mu\nabla^2\vec{V} + \rho\vec{g} + \vec{S}. \tag{2}$$

Here, ρ denotes the density of the mixture, V is the velocity vector, p is the pressure, μ is the dynamic viscosity, g is the gravitational acceleration, and S represents the momentum source term, defined as:

$$\vec{S} = -A(\gamma)\,\vec{V}, \tag{3}$$

Where:

$$A(\gamma) = \frac{C(1-\gamma)^2}{\gamma^3 + \varepsilon}. \tag{4}$$

A(γ), known as the porosity function. γ represents the liquid fraction of PCM in the computational cell, C is the mushy zone constant, and ε is a small numerical constant (ε = 0.001) to prevent division by zero.

III. Turbulence equations

ANSYS Fluent allows researchers to choose among several turbulence models. Turbulence occurs at the onset of simulation due to the moving interface between PCM and air. The RNG k-ε model was chosen for its superior stability. The transport equations for k (turbulent kinetic energy) and ε (its rate of dissipation) in the RNG k-ε model are as follows:

$$\frac{\partial}{\partial t}(\rho k) + \frac{\partial}{\partial x_i}(\rho k u_i) = \frac{\partial}{\partial x_j}\left(\alpha_k \mu_{eff}\frac{\partial k}{\partial x_j}\right) + G_k + G_b - \rho\varepsilon - Y_M + S_k. \tag{5}$$

$$\frac{\partial}{\partial t}(\rho\varepsilon) + \frac{\partial}{\partial x_i}(\rho\varepsilon u_i) = \frac{\partial}{\partial x_j}\left(\alpha_\varepsilon \mu_{eff}\frac{\partial \varepsilon}{\partial x_j}\right) + C_{1\varepsilon}\frac{\varepsilon}{k}(G_k + C_{3\varepsilon}G_b) - C_{2\varepsilon}\rho\frac{\varepsilon^2}{k} - R_\varepsilon + S_\varepsilon, \tag{6}$$

Where G_k represents the production of turbulent kinetic energy due to the gradients of the mean velocity. The turbulent kinetic energy generated by buoyancy effects is denoted by G_b. The contribution of oscillatory expansion in compressible turbulence to the overall dissipation rate is represented by Y_M. S_k and S_ϵ are user-

defined source terms. Finally, α_k and α_ϵ are the effective inverse Prandtl numbers for k and ϵ, respectively. The following formula shows how α_k and α_ϵ are analytically calculated based on the RNG theory:

$$\left|\frac{\alpha - 1.3929}{\alpha_0 - 1.3929}\right|^{0.6321} \left|\frac{\alpha + 2.3929}{\alpha_0 + 2.3929}\right|^{0.3679} = \frac{\mu_{mol}}{\mu_{eff}}. \quad (7)$$

It is assumed that α_0 equals 1. If the high Reynolds number condition is satisfied ($\mu_{mol}/\mu_{eff} \ll 1$), the values of α_k and α_ϵ are equal to 1.393. The model constants $C_{1\epsilon}$ and $C_{2\epsilon}$ are also analytically calculated based on the RNG theory. The values of the mentioned parameters are as follows:

$$C_{1\varepsilon} = 1.42. \quad (8)$$

$$C_{2\varepsilon} = 1.68. \quad (9)$$

IV. Multiphase equations and VOF model

As previously mentioned, the specific volume of PCM differs significantly between its solid and liquid states, causing volume changes during melting. The VOF model is used to capture these volumetric changes, with the volume fraction continuity equation expressed as:

$$\frac{1}{\rho_q}\left(\frac{\partial}{\partial t}(\alpha_q \rho_q) + \nabla.(\alpha_q \rho_q \vec{v}_q)\right) = S_{\alpha_q} + \sum_{p=1}^{n}(\dot{m}_{pq} - \dot{m}_{qp}). \quad (10)$$

Here, $\dot{m}_{pq}$ and $\dot{m}_{qp}$ represent the mass transfer rates between phases p and q.

The source term on the right-hand side of the equation, $S_{\alpha q}$, is considered zero here. It is noteworthy that in the VOF model, the volume fraction equation is not solved for the primary phase (the non-melting phase, in this case, air) and is instead calculated using the following formula:

$$\sum_{q=1}^{n} \alpha_q = 1. \quad (11)$$

V. Energy equation

$$\rho \frac{Dh}{Dt} = k\nabla^2 T. \quad (12)$$

The specific enthalpy is defined as the sum of the sensible enthalpies:

$$h_s = h_{ref} + \int_{T_{ref}}^{T} c_p\,(T)\,dt. \quad (13)$$

Here, h_{ref} represents the specific enthalpy at the reference temperature, and C_p is the specific heat capacity at constant pressure. Most PCMs melt over a temperature range rather than at a specific temperature. Specifically, when the temperature of the solid PCM exceeds the beginning of this range (known as the solidus temperature or T_S), the melting process begins, and it ends upon reaching the upper limit of this range (known as the liquidus temperature or T_L). At this point, no solid PCM remains. The enthalpy of the PCM significantly changes within this range.

To model this phenomenon, the parameter γ_L is used, where γ represents the fraction of PCM in the liquid state (during the phase change process, within the temperature range T_S=26∘C to T_L=28∘C in this study) and L is the latent heat of the PCM, assumed to be 179 kJ/kg. The mathematical formula for γ is defined as follows:

$$\gamma = \begin{cases} 0 & \text{if } T < T_S, \\ 1 & \text{if } T > T_L, \\ \dfrac{T - T_S}{T_L - T_S} & \text{if } T_S < T < T_L \end{cases}. \quad (14)$$

2.2.1 | Boundary conditions

The battery-PCM system was modeled in a vertical containment tube, as shown in *Fig. 3*. The PCM was initially in its solid phase, and the outer tube temperature was maintained at 40°C to simulate real-world heat dissipation. Initial and boundary conditions were applied as follows:

I. Initial temperature: 23°C for the battery, PCM, air, and aluminum tube.

II. Material properties: thermophysical properties of RT27 PCM, aluminum, and air were assigned based on *Table 1*.

III. No-slip wall conditions: applied to all solid surfaces.

IV. Natural convection at the top: PCM was open to air at the top for heat dissipation.

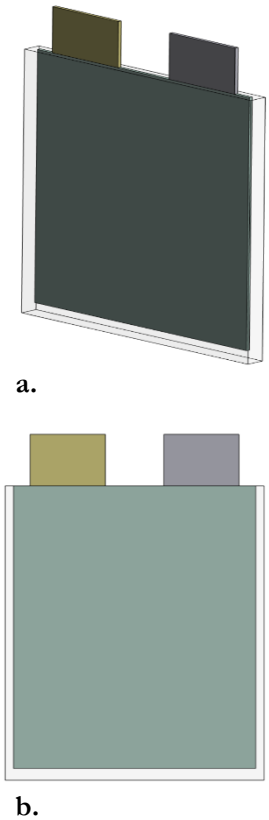

a.

b.

Fig. 3. Battery–PCM simulation model in ANSYS; a. Perspective view of the battery cell model within PCM material, and b. Front view of the battery cell and PCM material in ANSYS software.

Table 1. Thermophysical properties of RT27 and other materials.

Parameter	Value
Density of RT27 (PCM)	$\gamma = \begin{cases} 870 & T \le 299.15\ K \\ 781.5 & 299.15\ K \le T \le 301.15\ K \\ 750 & T \ge 301.15\ K \end{cases}$
Density of Aluminum (fins and tube)	2719 kg/m³
Specific heat capacity (RT27 PCM)	2500 J/(kg·K)
Specific heat capacity (air)	1006.43 J/(kg·K)
Specific heat capacity (Aluminum)	871 J/(kg·K)

Table 1. Continued.

Parameter	Value
Thermal conductivity (Solid phase)	0.24 W/(m·K)
Thermal conductivity (Liquid phase)	0.15 W/(m·K)
Thermal conductivity (Aluminum fins)	202.4 W/(m·K)
Latent heat of fusion (RT27 PCM)	179 kJ/kg
Solid phase transition temperature (RT27 PCM)	299.15 K
Liquid phase transition temperature (RT27 PCM)	301.15 K

A fine meshing strategy was implemented to ensure high-resolution thermal and fluid dynamics analysis, with 434,128 nodes and 1,705,392 elements, capturing intricate heat flow and phase transition behaviors.

2.3 | Simulation Setup

The thermal behavior of the battery cell integrated with PCMs was analyzed using ANSYS Fluent to assess heat dissipation efficiency and phase transition dynamics under different operating conditions. The simulation framework was designed to evaluate the influence of PCM integration on battery thermal performance, ensuring an accurate representation of heat generation, conduction, convection, and latent heat absorption.

To achieve reliable results, the numerical model incorporated a fine mesh resolution, well-defined initial and boundary conditions, and material properties derived from experimental data. Both steady-state and transient analyses were conducted to investigate temperature evolution, heat transfer mechanisms, and the impact of different discharge rates on battery performance.

V. Meshing and computational grid.

A structured computational grid was developed to accurately resolve thermal gradients and fluid interactions within the PCM domain. The meshing process was refined to balance computational efficiency and accuracy, ensuring sufficient resolution in regions with significant temperature variations. The final mesh consisted of:

Total nodes: 434,128.

Total elements: 1,705,392.

This high-density mesh allowed for detailed tracking of temperature distribution, phase change effects, and convection patterns within the PCM.

VI. Initial and boundary conditions.

The simulation was initialized with the following thermal and environmental conditions:

2.3.1 | Initial temperature

All system components, including the battery cell, PCM, aluminum tube, and surrounding air, were initialized at 23°C, with PCM entirely in its solid phase at the start of the simulation.

2.3.2 | Boundary conditions

The outer aluminum containment tube was maintained at 40°C, simulating heat dissipation in real-world applications. Natural convection was modeled at the top boundary using a pressure outlet condition to allow heat dissipation into the surrounding air. No-slip boundary conditions were applied to all solid surfaces, ensuring accurate modeling of conductive heat transfer between the battery, PCM, and containment tube.

2.3.3 | Material properties

The thermophysical properties of RT27 PCM and other materials were assigned based on *Table 1*, ensuring realistic thermal behavior representation in the simulations.

VII. Simulation type and approach

To evaluate the cooling performance of PCM-based thermal management, both steady-state and transient analyses were performed:

2.3.4 | Steady-state analysis

Provided an overview of the thermal equilibrium state, highlighting temperature distribution without dynamic phase change effects.

2.3.5 | Transient analysis

Captured time-dependent heat transfer phenomena, including PCM melting progression, latent heat absorption, and battery temperature variations over the discharge cycle.

VIII. Battery discharge rate and thermal load analysis

To analyze the impact of different discharge rates on battery thermal performance, simulations were performed for multiple C-rates, where 1C corresponds to a full battery discharge in one hour. *Table 2* presents the discharge rates along with their corresponding current values (A) and discharge times (s).

Table 2. Discharge rates, current values, and discharge times for the battery.

Discharge Rate	Current (A)	Time(s)
1C	2.5	3570
2C	5	1770
3C	7.5	1170
4C	10	870

This table highlights the inverse relationship between discharge rate and discharge time. As the discharge rate increases, the time required to deplete the battery fully decreases, leading to higher thermal loads due to increased current flow and Joule heating effects. These findings emphasize the importance of effective thermal management strategies, particularly under high-discharge conditions, to prevent excessive temperature rise and ensure battery safety and longevity.

3 | Results and Discussion

This section presents the thermal behavior of three different battery chemistries: LIB, Li-S, and SIB. The temperature distribution under static conditions was analyzed across various discharge rates (1C to 4C). *Figs. 4-7* illustrate these distributions, highlighting the influence of material properties on thermal performance.

3.1 | Thermal Behavior of Battery Materials

The static temperature distribution for three different battery chemistries is presented in *Fig. 4*. These figures illustrate the thermal response of LIB, Li-S, and SIB cells under similar operating conditions. The analysis highlights the influence of material properties on temperature distribution, which is critical for optimizing battery performance and safety.

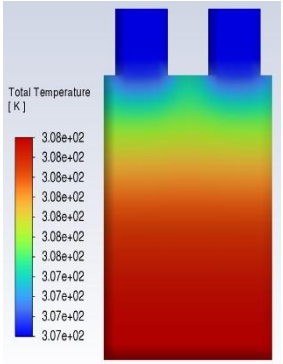

a.

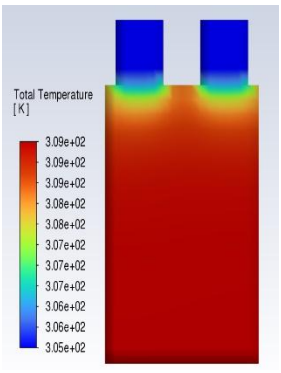

b.

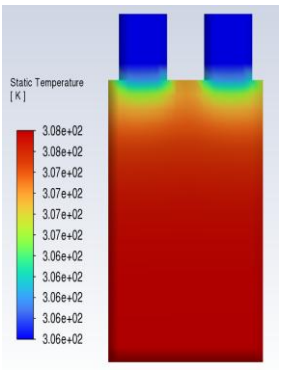

c.

Fig. 4. Static temperature distribution; a. LIB cell, b. Li-S battery cell, and c) SIB cell, (at a discharge rate of 1C).

Fig. 4 presents the static temperature distribution of three battery chemistries; a) LIB, b) Li-S, and c) SIB — at a discharge rate of 1C. The LIB battery exhibits a relatively uniform temperature distribution, with a narrow range from 307.0 K to 308.0 K, demonstrating its superior thermal conductivity and efficient heat dissipation. In contrast, the Li-S battery shows a wider temperature range, extending up to 309.0 K, with pronounced hotspots near the terminals. This non-uniformity is attributed to the material's lower thermal conductivity, which impedes effective heat distribution and increases thermal stress risks. Meanwhile, the SIB demonstrates exceptional thermal stability, with minimal temperature variation between 306.0 K and 307.0 K, highlighting its inherent thermal resilience and suitability for applications demanding consistent thermal performance. The comparative analysis in *Fig. 4* emphasizes the critical need for tailored thermal management solutions, especially for Li-S batteries, to address thermal hotspots and enhance system reliability.

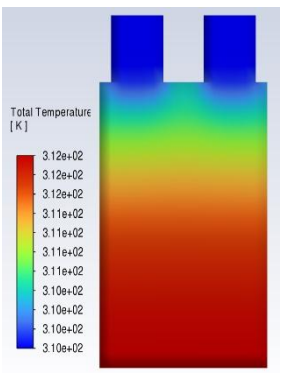

a.

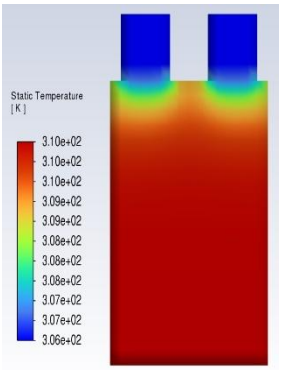

b.

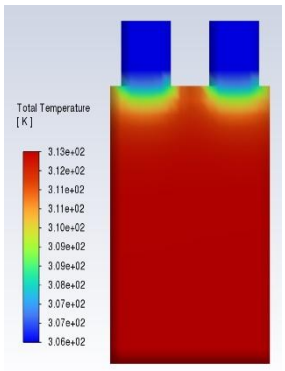

c.

Fig. 5. Static temperature distribution; a. LIB cell, b. Li-S battery cell, and c) SIB cell. At a discharge rate of 2C.

Fig. 5 illustrates the static temperature distribution of a) LIB, b) Li-S, and c) SIB cells at a discharge rate of (*Fig. 2.c)*. The LIB maintains a relatively uniform temperature profile ranging from 307.0 K to 312.0 K, reflecting efficient thermal conductivity and reliable heat dissipation under increased operational demands.

In contrast, the Li-S battery shows a wider temperature range, reaching up to 313.0 K, with evident hotspots near the terminals. This uneven temperature distribution highlights the material's lower thermal conductivity and the need for enhanced thermal management to prevent localized overheating. The SIB exhibits a more stable temperature profile, with a narrow range between 306.0 K and 310.0 K, confirming its superior thermal resilience even under higher discharge rates.

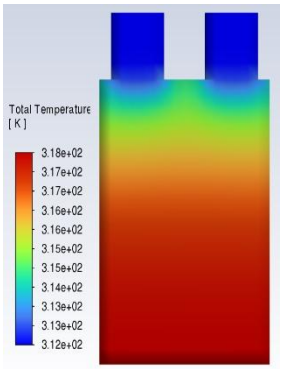

a.

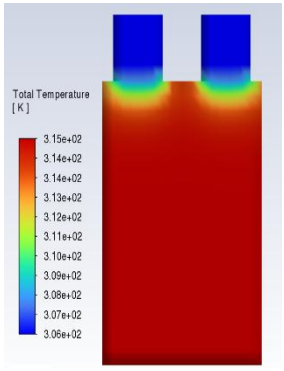

b.

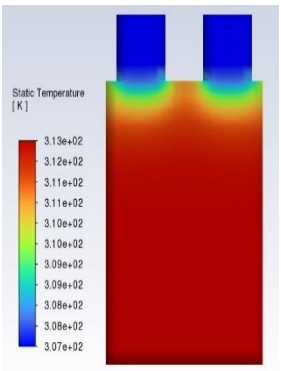

c.

Fig. 6. Static temperature distribution; a. LIB cell, b. Li-S battery cell, and c) SIB cell, (at a discharge rate of 3C).

Fig. 6 depicts the static temperature distribution for a) LIB, b) Li-S, and c) SIB cells at a discharge rate of (*Fig. 3.c)*. The LIB exhibits a relatively uniform temperature range from 312.0 K to 318.0 K, showcasing effective heat dissipation and maintaining a stable thermal profile under higher discharge rates.

However, the Li-S battery demonstrates a broader temperature range, with maximum temperatures reaching 315.0 K and pronounced hotspots near the terminals. This uneven distribution underscores the material's limitations in thermal conductivity, highlighting the need for robust thermal management strategies to prevent localized overheating and ensure operational safety. The SIB shows remarkable thermal stability, with temperatures ranging between 306.0 K and 313.0 K, further confirming its suitability for applications requiring consistent thermal performance.

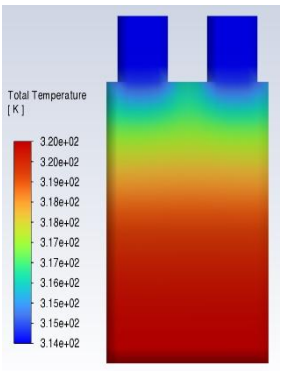

a.

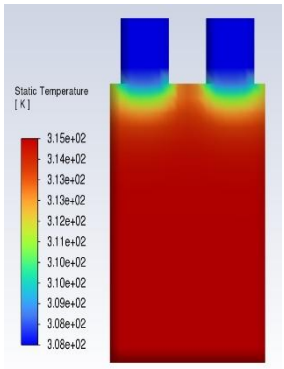

b.

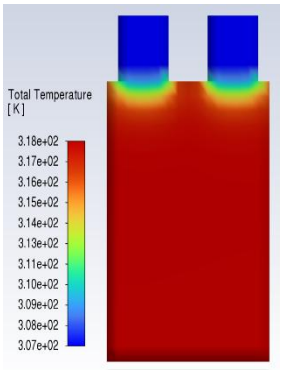

c.

Fig. 7. Static temperature distribution; a. LIB cell, b. Li-S battery cell, and c) SIB cell. (at a discharge rate of 4C).

Fig. 7 displays the static temperature distribution of a) LIB, b) Li-S, and c) SIB cells at a discharge rate of (*Fig. 4.c)*. The LIB demonstrates a temperature range between 314.0 K and 320.0 K, maintaining relative uniformity despite the higher thermal load, indicating its ability to handle increased discharge rates efficiently. Conversely, the Li-S battery shows a significant rise in temperature, with values extending up to 317.0 K and prominent hotspots near the terminals. It highlights the material's inadequate thermal conductivity and the critical need for enhanced cooling to prevent localized overheating. The SIB, however, maintains its thermal stability with a narrow temperature range of 308.0 K to 315.0 K, showcasing its inherent ability to regulate heat effectively even under demanding conditions.

The analysis of *Figs. 4-7* reveals the growing thermal challenges in different battery chemistries under increasing discharge rates (1C to 4C). LIB exhibit a relatively uniform temperature distribution and efficient heat dissipation; however, their peak temperatures rise significantly at higher discharge rates, necessitating robust thermal management. In contrast, Li-S batteries show wider temperature ranges and prominent hotspots near terminals, reflecting poor thermal conductivity and higher risks of thermal stress and degradation. SIB maintain stable thermal profiles with minimal gradients, but their performance could still benefit from improved heat dissipation at high rates. The increasing temperature and uneven distribution at higher discharge rates highlight the need for PCMs. PCMs effectively absorb and redistribute heat, reducing thermal gradients, minimizing hotspots, and ensuring temperature uniformity. By integrating PCMs, battery systems can operate more safely and efficiently, extending their lifespan and mitigating risks of thermal runaway, especially for chemistries like Li-S that are more thermally vulnerable.

3.2 | Phase Change Materials Cooling System Efficiency

In this section, the efficiency of the PCM cooling system is evaluated by analyzing the thermal behavior of the battery cells with PCM integrated at various discharge rates (1C to 4C). *Figs. 8-11* depict the static temperature distribution for each battery chemistry (LIB, Li-S, and SIB) at increasing discharge rates,

providing a clear picture of how PCM affects temperature uniformity and heat dissipation across different operating conditions. The static temperature distribution at a discharge rate of 1C, shown in *Fig. 8*, highlights the differences in thermal behavior across three battery chemistries. The LIB (*Fig. 8.a*) exhibits a relatively narrow temperature range, from 307.0 K to 308.0 K, indicating efficient heat dissipation and effective performance of the PCM cooling system. This uniform temperature distribution is a result of LIB high thermal conductivity, allowing for even heat spread across the surface of the battery. In contrast, the Li-S battery (*Fig. 8.b*) shows a wider temperature range, with hotspots reaching up to 309.0 K, especially near the terminals. This uneven distribution is caused by the lower thermal conductivity of Li-S, which hinders efficient heat distribution, leading to localized overheating. The PCM system offers some cooling but is less effective in managing the thermal stress associated with Li-S's poor heat conductivity. The SIB (*Fig. 8.c*), however, demonstrates superior thermal stability with minimal temperature variation, ranging from 306.0 K to 307.0 K, underscoring the battery's inherent thermal resilience even under the moderate load of 1C. This stability highlights the effectiveness of the PCM system in maintaining uniform temperatures for SIB.

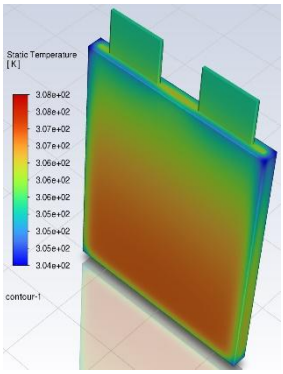

a.

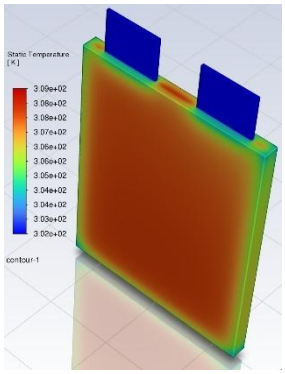

b.

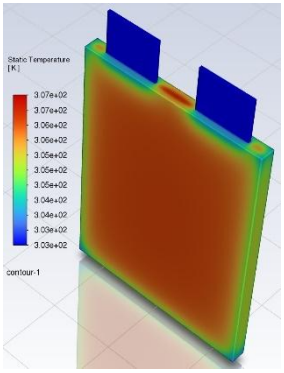

c.

Fig. 8. Static temperature distribution; a. LIB cell: b. Li-S battery cell and c. SIB cell, (at a discharge rate of 1C).

At a discharge rate of 2C, as shown in *Fig. 9*, the LIB (*Fig. 9.a*) shows a temperature range from 307.0 K to 312.0 K, indicating effective heat dissipation with a slight increase in temperature compared to 1C. The PCM system continues to work well, but higher discharge rates highlight the need for monitoring to ensure temperatures stay within safe limits. In contrast, the Li-S battery (*Fig. 9.b*) exhibits a broader temperature range, reaching 313.0 K, with noticeable hotspots near the terminals. It indicates that the PCM cooling system struggles to manage heat effectively due to the low thermal conductivity of Li-S, requiring enhanced cooling solutions to prevent thermal stress.The SIB (*Fig. 9.c*) remains thermally stable, with a temperature range of 306.0 K to 310.0 K, demonstrating consistent thermal performance even under higher discharge rates. It suggests that SIB, combined with PCM cooling, offer superior thermal stability compared to other chemistries. Overall, PCM cooling effectively supports LIB and SIB. However, Li-S batteries face significant challenges in maintaining thermal uniformity under higher discharge rates, necessitating further optimization of cooling strategies.

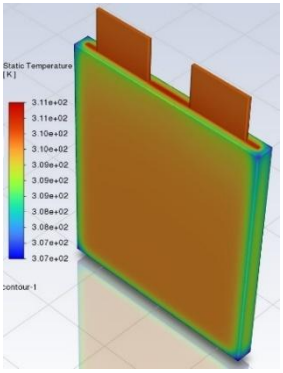

a.

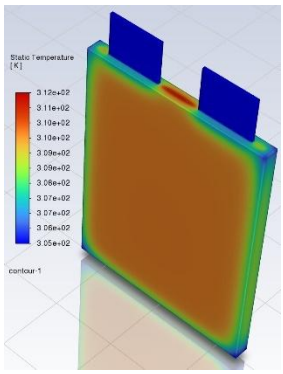

b.

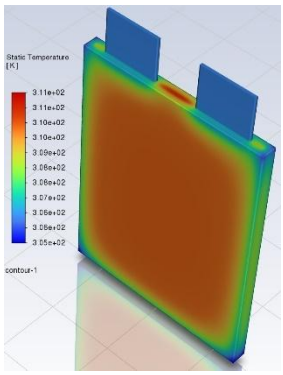

c.

Fig. 9. Static temperature distribution: a. LIB cell, b. Li-S battery cell and c. SIB cell. At a discharge rate of 2C.

At a discharge rate of 3C (*Fig. 10*), the LIB (*Fig. 10.a*) shows a temperature range between 312.0 K and 318.0 K, with some increased temperature variation compared to the previous rates. While the PCM system still

performs well in maintaining temperature stability, the higher discharge rate leads to a noticeable increase in peak temperatures, signaling the need for more advanced cooling strategies at higher loads. The Li-S battery (*Fig. 10.b*), however, presents a significant thermal challenge with a temperature range extending up to 315.0 K, accompanied by hotspots near the terminals. This issue arises due to the lower thermal conductivity of Li-S, which hinders the uniform heat distribution, leading to localized overheating and highlighting the insufficiency of the PCM cooling system under these conditions.

In contrast, the SIB (*Fig. 10.c*) maintains superior thermal stability, with a narrow temperature range from 306.0 K to 313.0 K. This consistent performance, even at 3C, underscores the thermal resilience of SIB ries and the effective role of PCM in stabilizing temperatures even under high discharge rates. While SIB perform optimally, the Li-S batteries clearly demonstrate the need for further optimization of the PCM cooling system to reduce thermal gradients and improve heat dissipation, especially when dealing with higher discharge rates. This analysis reinforces the need for targeted cooling improvements for chemistries with lower thermal conductivity.

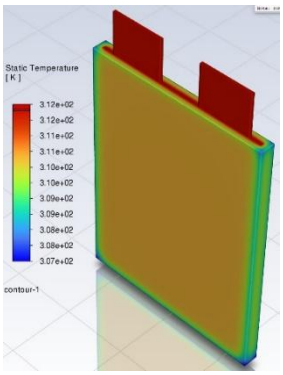

a.

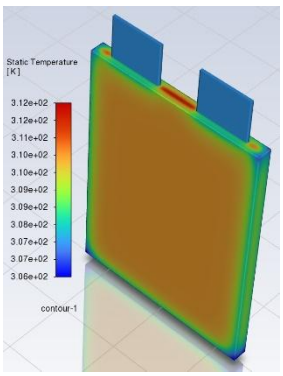

b.

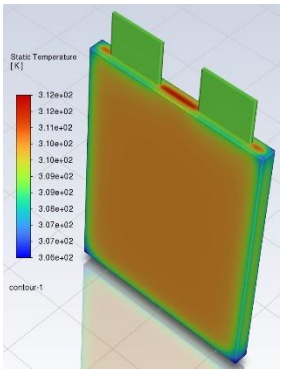

c.

Fig. 10. Static temperature distribution; a. LIB cell, b. Li-S battery cell, and c. SIB cell. (at a discharge rate of 3C).

At a discharge rate of 4C (*Fig. 11*), the LIB (*Fig. 11.a*) shows an increase in temperature range, from 314.0 K to 320.0 K, but the temperature distribution remains relatively uniform. The PCM cooling system continues to effectively moderate the heat generated by the battery, though the higher discharge rate introduces more thermal load. Despite this, the LIB manages to maintain its temperature within a safe range, though continuous monitoring will be required to ensure performance under even higher discharge conditions. On the other hand, the Li-S battery (*Fig. 11.b*) exhibits a wider temperature range, reaching up to 317.0 K, with pronounced hotspots near the terminals. It highlights the poor thermal conductivity of Li-S, which hampers the PCM's ability to dissipate heat efficiently, especially under high discharge rates. These results emphasize the need for improved PCM design or additional cooling solutions for Li-S batteries to mitigate thermal stress and prevent degradation.

In contrast, the SIB (*Fig. 11.c*) demonstrates excellent thermal stability with a temperature range from 308.0 K to 315.0 K, even at the high 4C discharge rate. This stable temperature profile indicates that SIB are thermally resilient, and the PCM cooling system is highly effective in maintaining uniform heat distribution. While SIB perform optimally at high discharge rates, Li-S batteries require further optimization in their TMS to handle the increasing heat load. The results reinforce the importance of tailored cooling solutions for each battery chemistry, particularly for Li-S, where the battery's low thermal conductivity limits PCM performance.

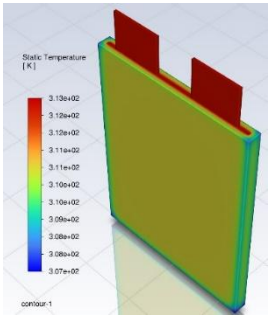

a.

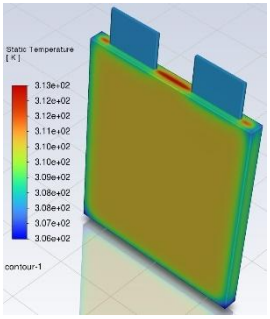

b.

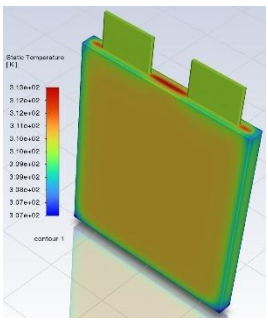

c.

Fig. 11. Static temperature distribution;
a. LIB cell, b. Li-S battery cell, c. SIB cell.
(at a discharge rate of 4C).

In conclusion, the results from *Figs. 8-11* demonstrate significant differences in the thermal performance of the three battery chemistries under increasing discharge rates from 1C to 4C. LIB exhibit relatively stable temperature distributions, with the PCM cooling system performing effectively, though higher discharge rates reveal an increased need for more advanced cooling solutions. Li-S batteries, on the other hand, face considerable thermal challenges, with wider temperature ranges and hotspot formation, highlighting the limitations of their thermal conductivity and the need for optimized cooling strategies. In contrast, SIB showcase remarkable thermal stability across all discharge rates, with the PCM system proving highly effective at maintaining consistent temperature regulation. These findings underscore the importance of tailored TMS, particularly for Li-S batteries, to ensure safe and efficient operation, while SIB emerge as a promising candidate for applications requiring robust thermal performance under demanding conditions.

4 | Conclusion

This study aimed to investigate the thermal performance of different battery chemistries— LIB, Li-S, and SIB—with a focus on the role of PCMs in managing heat dissipation at varying discharge rates.

The results highlight several key findings:

I. LIB demonstrate relatively stable thermal behavior, with PCM systems effectively managing heat at lower discharge rates. However, as discharge rates increase, the thermal load also rises, suggesting that advanced cooling strategies are necessary for optimal performance at higher discharge rates.

II. Li-S batteries show significant thermal challenges, particularly due to their lower thermal conductivity. It leads to localized overheating and hotspot formation, especially under high discharge rates. Thus, enhanced PCM designs or additional cooling mechanisms are crucial for improving thermal uniformity and preventing thermal degradation.

III. SIB, in contrast, exhibit superior thermal stability, with PCM systems effectively managing heat dissipation across a broad range of operating conditions. The inherent thermal resilience of SIB at high discharge rates makes them a promising alternative for applications requiring consistent thermal performance.

The study emphasizes the importance of developing tailored TMS based on the specific thermal behavior and material properties of each battery chemistry. While Li-S batteries face notable challenges in heat distribution, SIB show significant potential for high-performance applications due to their superior thermal resilience.

For future research, it is essential to focus on optimizing PCM materials specific to each battery chemistry, exploring hybrid cooling solutions, and examining the real-world applications of these systems in different operating conditions. Addressing these thermal management challenges will enhance the efficiency, safety, and longevity of next-generation batteries, paving the way for more sustainable and reliable energy storage technologies.

Acknowledgments

The authors sincerely thank all those who contributed to this research through their guidance, expertise, and helpful recommendations.

Funding

No funding was received for this research.

Data Availability

Relevant data supporting the conclusions of this study can be obtained from the corresponding author upon reasonable request.

References

[1] Salami, R. Y., Shojaeefard, M. H., Molaeimanesh, G. R. (2018). Thermal behavior of a commercial prismatic Lithium-Ion battery cell applied in electric vehicles. *International journal of automotive engineering*, *8*(2), 2700–2708. http://dx.doi.org/10.22068/ijae.8.2.2700

[2] Ni, D., Xiao, Z., & Lim, M. K. (2020). A systematic review of the research trends of machine learning in supply chain management. *International journal of machine learning and cybernetics*, *11*, 1463–1482. https://doi.org/10.1007/s13042-019-01050-0

[3] Baccouche, I., Jemmali, S., Manai, B., Nikolian, A., Omar, N., & Essoukri Ben Amara, N. (2022). Li-ion battery modeling and characterization: An experimental overview on NMC battery. *International journal of energy research*, *46*(4), 3843–3859. https://doi.org/10.1002/er.7445

[4] Guo, J., Li, Y., Pedersen, K., & Stroe, D. I. (2021). Lithium-Ion battery operation, degradation, and aging mechanism in electric vehicles: An overview. *Energies*, *14*(17), 5220. https://doi.org/10.3390/en14175220

[5] Chen, S. C., Wan, C. C., & Wang, Y. Y. (2005). Thermal analysis of lithium-ion batteries. *Journal of power sources*, *140*(1), 111–124. https://doi.org/10.1016/j.jpowsour.2004.05.064

[6] Shen, H., Wang, H., Li, M., Li, C., Zhang, Y., Li, Y., … & Ouyang, M. (2023). Thermal runaway characteristics and gas composition analysis of lithium-ion batteries with different LFP and NCM cathode materials under inert atmosphere. *Electronics*, *12*(7), 1603. https://doi.org/10.3390/electronics12071603

[7] Deng, Z., Hu, X., Lin, X., Kim, Y., & Li, J. (2021). Sensitivity analysis and joint estimation of parameters and states for all-solid-state batteries. *IEEE transactions on transportation electrification*, *7*(3), 1314–1323. https://doi.org/10.1109/TTE.2021.3050987

[8] Tran, M.-K., DaCosta, A., Mevawalla, A., Panchal, S., & Fowler, M. (2021). Comparative study of equivalent circuit models performance in four common lithium-ion batteries: LFP, NMC, LMO, NCA. *Batteries*, *7*(3), 51. https://doi.org/10.3390/batteries7030051

[9] Fotouhi, A., Auger, D. J., Propp, K., Longo, S., & Wild, M. (2016). A review on electric vehicle battery modelling: From lithium-ion toward lithium–sulphur. *Renewable and sustainable energy reviews*, *56*, 1008–1021. https://doi.org/10.1016/j.rser.2015.12.009

[10] Chen, Y., Wang, T., Tian, H., Su, D., Zhang, Q., & Wang, G. (2021). Advances in lithium--sulfur batteries: from academic research to commercial viability. *Advanced materials*, *33*(29), 2003666. https://doi.org/10.1002/adma.202003666

[11] Yang, X., Li, X., Adair, K., Zhang, H., & Sun, X. (2018). Structural design of lithium–sulfur batteries: From fundamental research to practical application. *Electrochemical energy reviews*, *1*(3), 239–293. https://doi.org/10.1007/s41918-018-0010-3

[12] Jin, B., Kim, J. U., & Gu, H. B. (2003). Electrochemical properties of lithium–sulfur batteries. *Journal of power sources*, *117*(1), 148–152. https://doi.org/10.1016/S0378-7753(03)00113-7

[13] Yu, W., Deng, N., Cheng, K., Yan, J., Cheng, B., & Kang, W. (2021). Advances in preparation methods and mechanism analysis of layered double hydroxide for lithium-ion batteries and lithium-sulfur batteries. *Journal of energy chemistry*, *58*, 472–499. https://doi.org/10.1016/j.jechem.2020.10.031

[14] Andrei, P., Shen, C., & Zheng, J. P. (2018). Theoretical and experimental analysis of precipitation and solubility effects in lithium-sulfur batteries. *Electrochimica acta*, *284*, 469–484. https://doi.org/10.1016/j.electacta.2018.07.045

[15] Chung, S. H., Chang, C. H., & Manthiram, A. (2018). Progress on the critical parameters for lithium--sulfur batteries to be practically viable. *Advanced functional materials*, *28*(28), 1801188. https://doi.org/10.1002/adfm.201801188

[16] Nekahi, A., Dorri, M., Rezaei, M., Bouguern, M. D., Madikere Raghunatha Reddy, A. K., Li, X., … & Zaghib, K. (2024). Comparative issues of metal-ion batteries toward sustainable energy storage: Lithium vs. Sodium. *Batteries*, *10*(8), 279. https://doi.org/10.3390/batteries10080279

[17] Duffner, F., Kronemeyer, N., Tübke, J., Leker, J., Winter, M., & Schmuch, R. (2021). Post-lithium-ion battery cell production and its compatibility with lithium-ion cell production infrastructure. *Nature energy*, *6*(2), 123–134. https://doi.org/10.1038/s41560-020-00748-8

[18] Adelhelm, P., Hartmann, P., Bender, C. L., Busche, M., Eufinger, C., & Janek, J. (2015). From lithium to sodium: cell chemistry of room temperature sodium--air and sodium--sulfur batteries. *Beilstein journal of nanotechnology*, *6*(1), 1016–1055. https://doi.org/10.3762/bjnano.6.105

[19] Hou, D., Xia, D., Gabriel, E., Russell, J. A., Graff, K., Ren, Y., … & Xiong, H. (2021). Spatial and temporal analysis of sodium-ion batteries. *ACS energy letters*, *6*(11), 4023–4054. https://doi.org/10.1021/acsenergylett.1c01868

[20] Kharabati, S., & Saedodin, S. (2024). A systematic review of thermal management techniques for electric vehicle batteries. *Journal of energy storage*, *75*, 109586. https://doi.org/10.1016/j.est.2023.109586

[21] Dai, Q., Kelly, J. C., Gaines, L., & Wang, M. (2019). Life cycle analysis of lithium-ion batteries for automotive applications. *Batteries*, *5*(2), 48. https://doi.org/10.3390/batteries5020048

[22] Kim, J., Oh, J., & Lee, H. (2019). Review on battery thermal management system for electric vehicles. *Applied thermal engineering*, *149*, 192–212. https://doi.org/10.1016/j.applthermaleng.2018.12.020

[23] Tete, P. R., Gupta, M. M., & Joshi, S. S. (2021). Developments in battery thermal management systems for electric vehicles: A technical review. *Journal of energy storage*, *35*, 102255. https://doi.org/10.1016/j.est.2021.102255

[24] Liang, J., Gan, Y., Yao, M., & Li, Y. (2021). Numerical analysis of capacity fading for a LiFePO4 battery under different current rates and ambient temperatures. *International journal of heat and mass transfer*, *165*, 120615. https://doi.org/10.1016/j.ijheatmasstransfer.2020.120615

[25] Javani, N., Dincer, I., Naterer, G. F., & Rohrauer, G. L. (2014). Modeling of passive thermal management for electric vehicle battery packs with PCM between cells. *Applied thermal engineering*, *73*(1), 307–316. https://doi.org/10.1016/j.applthermaleng.2014.07.037

[26] Lyu, P., Liu, X., Qu, J., Zhao, J., Huo, Y., Qu, Z., & Rao, Z. (2020). Recent advances of thermal safety of lithium ion battery for energy storage. *Energy storage materials*, *31*, 195–220. https://doi.org/10.1016/j.ensm.2020.06.042

[27] Salami, Y., Aghabeigi, M., & Imani, F. (2021). A Review on Electric Vehicle Battery Thermal Management Systems, Merits, and Demerits. In *8th conference on thermal power plants, toosi university of technology, Tehran, Iran*. 25-27. https://www.researchgate.net

[28] Xu, B., Oudalov, A., Ulbig, A., Andersson, G., & Kirschen, D. S. (2016). Modeling of lithium-ion battery degradation for cell life assessment. *IEEE transactions on smart grid*, *9*(2), 1131–1140. https://doi.org/10.1109/TSG.2016.2578950

[29] Deng, Z., Zhang, Z., Lai, Y., Liu, J., Li, J., & Liu, Y. (2013). Electrochemical impedance spectroscopy study of a Lithium/Sulfur battery: Modeling and analysis of capacity fading. *Journal of the electrochemical society*, *160*(4), A553. https://doi.org/10.1149/2.026304jes

[30] Cañas, N. A., Fronczek, D. N., Wagner, N., Latz, A., & Friedrich, K. A. (2014). Experimental and theoretical analysis of products and reaction intermediates of Lithium–Sulfur batteries. *The journal of physical chemistry c*, *118*(23), 12106–12114. https://doi.org/10.1021/jp5013208

[31] Bhargav, A., He, J., Gupta, A., & Manthiram, A. (2020). Lithium-Sulfur batteries: Attaining the critical metrics. *Joule*, *4*(2), 285–291. https://doi.org/10.1016/j.joule.2020.01.001

[32] Jayasinghe, A. E., Fernando, N., Kumarawadu, S., & Wang, L. (2023). Review on li-ion battery parameter extraction methods. *IEEE access*, *11*, 73180–73197.

[33] Xue, N. (2014). *Design and optimization of lithium-ion batteries for electric-vehicle applications* [Thesis]. https://deepblue.lib.umich.edu/bitstreams/8f06f70d-a6f8-4f39-ad2f-bba531ceff43/download

[34] Lin, J., Liu, X., Li, S., Zhang, C., & Yang, S. (2021). A review on recent progress, challenges and perspective of battery thermal management system. *International journal of heat and mass transfer*, *167*, 120834. https://doi.org/10.1016/j.ijheatmasstransfer.2020.120834

[35] Del Valle, J. A., Anseán, D., Viera, J. C., Antuña, J. L., González, M., & Garc'ia, V. (2018). Analysis of advanced lithium-ion batteries for battery energy storage systems. *2018 ieee international conference on environment and electrical engineering and 2018 IEEE industrial and commercial power systems europe (EEEIC/I\&CPS Europe)* (pp. 1–6). IEEE. https://doi.org/10.1109/EEEIC.2018.8493934

[36] Liu, Y., Zheng, R., & Li, J. (2022). High latent heat phase change materials (PCMs) with low melting temperature for thermal management and storage of electronic devices and power batteries: Critical review. *Renewable and sustainable energy reviews*, *168*, 112783. https://doi.org/10.1016/j.rser.2022.112783

[37] Jilte, R., Afzal, A., & Panchal, S. (2021). A novel battery thermal management system using nano-enhanced phase change materials. *Energy*, *219*, 119564. https://doi.org/10.1016/j.energy.2020.119564

[38] Bahramian, S., & Ranjbaran, Y. S. (2021). Thermal behavior enhancement of battery thermal management systems based on phase change materials via a multitude of strategies. *10th international conference on new solutions in engineering, information science and technology of the century aheadat: Tehran, Iran*. https://www.researchgate.net

[39] Ranjbaran, Y. S., Imani, F., & Aghabeigi, M. (2021). Improving the thermal performance of PCM-based battery thermal management system applied in green vehicles. In *7th international conference on mechanical, construction, industrial and civil engineering*. 1-10. Civilica. https://en.civilica.com/doc/1230855/

[40] Mohammed, A. G., Elfeky, K. E., & Wang, Q. (2022). Recent advancement and enhanced battery performance using phase change materials based hybrid battery thermal management for electric vehicles. *Renewable and sustainable energy reviews*, *154*, 111759. https://doi.org/10.1016/j.rser.2021.111759

[41] Chen, J., Kang, S., E, J., Huang, Z., Wei, K., Zhang, B., … & Liao, G. (2019). Effects of different phase change material thermal management strategies on the cooling performance of the power lithium ion batteries: A review. *Journal of power sources*, *442*, 227228. https://doi.org/10.1016/j.jpowsour.2019.227228

[42] Ranjbaran, Y. S., Shojaeefard, M. H., & Molaeimanesh, G. R. (2023). Thermal performance enhancement of a passive battery thermal management system based on phase change material using cold air passageways for lithium batteries. *Journal of energy storage*, *68*, 107744. https://doi.org/10.1016/j.est.2023.107744

[43] Shojaeefard, M. H., Molaeimanesh, G. R., & Ranjbaran, Y. S. (2019). Improving the performance of a passive battery thermal management system based on PCM using lateral fins. *Heat and mass transfer*, *55*(6), 1753–1767. https://doi.org/10.1007/s00231-018-02555-0

Appendix

C	Mushy zone number in Eq. (4) (kg/ (m³.s))
g	Gravitational acceleration (m/s²)
G_b	Turbulence kinetic energy generation by buoyancy forces (kg/ (m.s³))
G_k	Turbulence kinetic energy generation caused by mean velocity gradients (kg/ (m.s³))
h	Specific enthalpy (J/kg)
k	Thermal conductivity (W/ (m.K))
L	Latent heat for phase change material (J/kg)
$\dot{m}_{pq}$	Mass transfer rate from phase p to phase q (kg/s)
$\dot{m}_{qp}$	Mass transfer from phase q to phase p (kg/s)
p	Pressure (Pa)
S	Source term
t	Time (s)
T	Temperature (K)
u_i	ith component of velocity vector (m/s)
	Velocity vector (m/s)

Greek symbols

α	Volume fraction
γ	Liquid fraction
μ	Dynamic viscosity (kg/ (m.s))
ρ	Density (kg/m³)

Subscripts

b	Buoyancy
eff	Effective
L	Liquidus
ref	Reference value
s	Solidus / sensible
b	Buoyancy

Acronyms

BEV	Battery electric vehicle
BTMS	Battery thermal management system
CENG	Compressed extended natural graphite
FCEV	Fuel cell electric vehicle
HEV	Hybrid electric vehicle
PCM	Phase change material
RNG	Renormalized group
VOF	Volume of fluid